Supplement to: Understanding Changes in Iceland's Streamflow Dynamics in Response to Climate Change

Hordur B. Helgason[1,2], Andri Gunnarsson[2], Óli G. B. Sveinsson[2], Bart Nijssen[1]

[1]Department of Civil and Environmental Engineering, University of Washington, Seattle, USA
[2]Hydropower Division, Landsvirkjun, Reykjavík, Iceland

Correspondence to: Hordur B. Helgason (helgason@uw.edu)

S1 Homogeneity analysis of streamflow series

To assess the homogeneity of streamflow records from the LamaH-Ice dataset, we performed the standard Pettitt's test (Pettitt, 1979). Our approach to considering or omitting inhomogeneous series aligns with that of the Norwegian Water Resources and Energy Directorate's method for selecting reference streamflow series for climate change studies (Fleig et al., 2013). The homogeneity analysis revealed that one timeseries needed to be omitted (Syðri-Bægisá river). The analysis, including the justification for each streamflow series, is described here.

Pettitt's test (Pettitt, 1979) is a non-parametric change-point detection test derived from the Mann-Whitney two-sample test. We computed Pettitt's test for each streamflow gauge using the PyHomogeneity Python package (Hussain et al., 2023), setting the significance level at 0.05 and the number of Monte Carlo simulations used to approximate the significance of the test at 20,000. We applied the test to series for annual average streamflow, temperature and precipitation series. In cases where the test indicated a change-point in annual average streamflow, we manually inspected the streamflow series for breaks in homogeneity that were either 1) linked to a documented change in measurement practices or to incidents that compromised data quality, or 2) distinctly observable in the data, and these breaks could not be accounted for by breaks in temperature or precipitation.

S2 Validity of trends in ERA5-Land

Temperature:

To assess the suitability of ERA5-Land for long-term temperature trend analysis in Iceland, we compared reanalysis-derived temperature series with in-situ observations from the Reykjavík weather station. The selected catchment, Korpa River (ID 58), is located in Reykjavík, with the streamflow gauge situated approximately 7 km from the weather station.

Figure S1: Comparison of observed temperature series in Reykjavík and catchment-averaged ERA5-Land series for the Korpa catchment (ID 58), located near Reykjavík, over the 1974–2023 period. The top panel shows monthly mean temperatures, and the bottom panel displays annual mean temperatures with Theil-Sen trend lines and associated p-values based on the modified Mann-Kendall test.

The comparison reveals excellent agreement between ERA5-Land and observed monthly temperature series, with a Pearson correlation coefficient of 0.994. Annual mean temperatures also show strong agreement (r = 0.975). Both datasets exhibit statistically significant warming over the 50-year study period. The Theil-Sen slope estimates indicate a warming trend of 0.42°C per decade for ERA5-Land and 0.35°C per decade for observations, both with p-values < 0.001. The temperature series from ERA5-Land is slightly cooler than the observed series, reflecting the higher average elevation of the catchment (171 m a.s.l.) compared to the weather station elevation (60 m a.s.l.). These findings confirm that ERA5-Land effectively captures interannual variability and long-term temperature trends at this site, supporting its use in hydrological and climate analyses across Iceland.

To assess potential temperature biases in ERA5-Land, we compared its mean annual temperature over the period 1973–2018 with that of the regional atmospheric reanalysis RAV-II**.** The comparison was performed for 111 catchments in the LamaH-Ice dataset, and results are presented in Figure S2

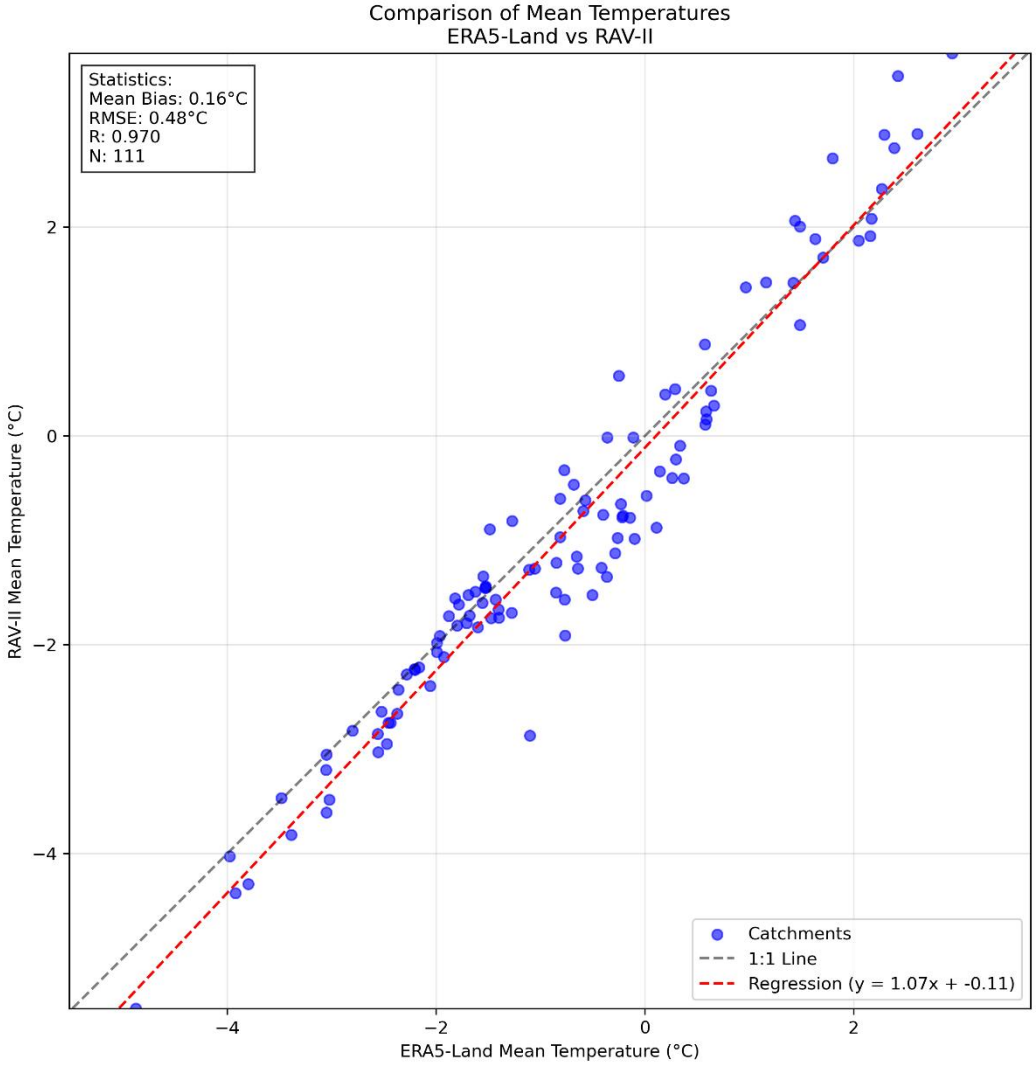

Figure S2: Comparison of mean annual temperatures between ERA5-Land and RAV-II reanalysis datasets for 111 catchments in LamaH-Ice during the period Oct 1 1973 – Sept 30 2018. The gray dashed line represents the 1:1 relationship, while the red dashed line shows the linear regression (y = 1.07x - 0.11). Each point represents one catchment, with temperatures ranging from approximately -4°C to +3°C.

ERA5-Land exhibits a slight warm bias compared to RAV-II, with a mean difference of +0.16°C, a root mean squared error (RMSE) of 0.48°C, and a pearson correlation coefficient of 0.97. The bias is temperature-dependent: ERA5-Land tends to be slightly colder than RAV-II at low temperatures (below –1.5°C), and slightly warmer at higher temperatures. Despite this

minor systematic difference, the strong agreement between the two datasets supports the suitability of ERA5-Land for analyzing long-term temperature trends in Iceland.

Precipitation:

Direct comparisons between reanalysis-based precipitation estimates and gauge observations in cold regions are challenging due to significant measurement uncertainties, particularly undercatch during snowfall and windy conditions. Because systematic corrections are not uniformly applied to Icelandic precipitation records, station-based trends may not provide a reliable reference for evaluating reanalysis products.

To assess the validity of ERA5-Land precipitation trends, we compared them with trends derived from the Copernicus Arctic Regional Reanalysis (CARRA), a high-resolution (2.5x2.5 km) regional reanalysis. Figure S3 presents precipitation trends (% per decade) from both ERA5-Land (left) and CARRA (center) over the 1993–2023 period, alongside a scatter plot comparing trends between the two datasets (right). Trends were computed using the Theil-Sen estimator.

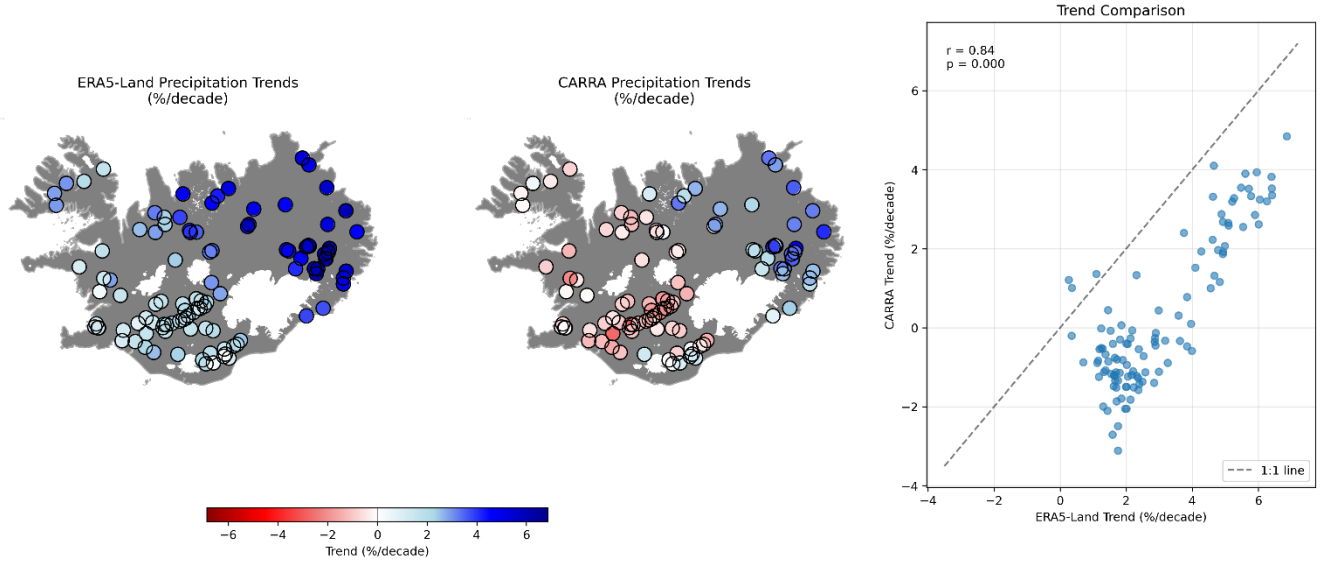

Figure S3: Comparison of precipitation trends (% per decade) over Iceland for the 1993–2023 period from ERA5-Land (left) and CARRA (center). Each point represents a catchment in the LamaH-Ice dataset. Trends were estimated using the Theil-Sen slope. The right panel shows a scatter plot comparing ERA5-Land and CARRA trends, with the dashed 1:1 line indicating perfect agreement.

Both datasets show broadly consistent spatial patterns in precipitation trends across Iceland. In particular, both reanalyses indicate increasing precipitation trends in the east and northeast, transitioning to decreasing or near-zero trends toward the southwest. This spatial coherence strengthens confidence in the qualitative pattern of change. However, ERA5-Land generally exhibits larger trend magnitudes than CARRA. This is reflected in the scatter plot, where most points fall below the 1:1 line, indicating that ERA5-Land trends are consistently higher than those from CARRA. The correlation between the two datasets is strong ($r = 0.84$, $p < 0.001$), suggesting a high level of agreement in relative trend patterns, even if the magnitudes differ.

These results suggest that ERA5-Land captures the broad spatiotemporal distribution of precipitation trends in Iceland and is suitable for use in large-scale hydrological trend assessments, such as those in LamaH-Ice.

S3 Changes in evapotranspiration compared to changes in precipitation

Figure S4 shows a comparison between trends in precipitation and ET in Iceland.

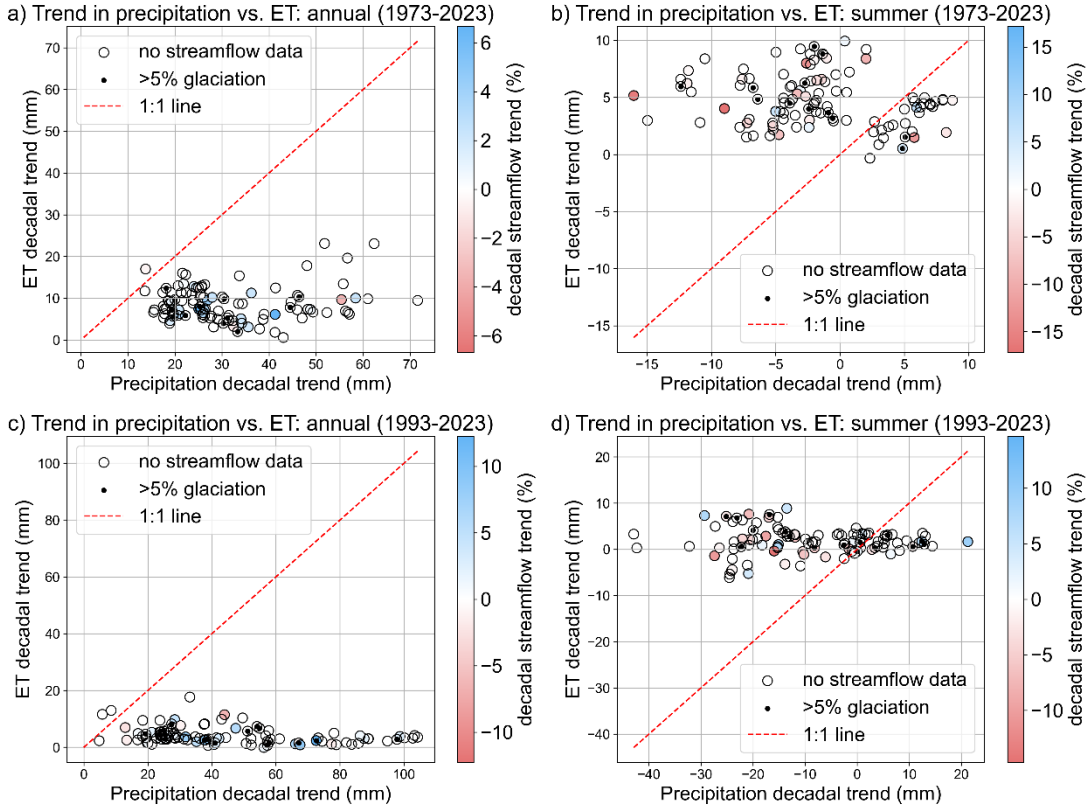

Figure S4: The trend in precipitation (x-axis) plotted against the trend for evapotranspiration (ET: y-axis) for period 1 (a and b) and period 2 (c and d). Annual trends are shown in panels a and c, summer trends (JJA) are shown in panels b and d. Colors indicate streamflow trends.

S4 Sub-seasonal trends in temperature, precipitation and streamflow

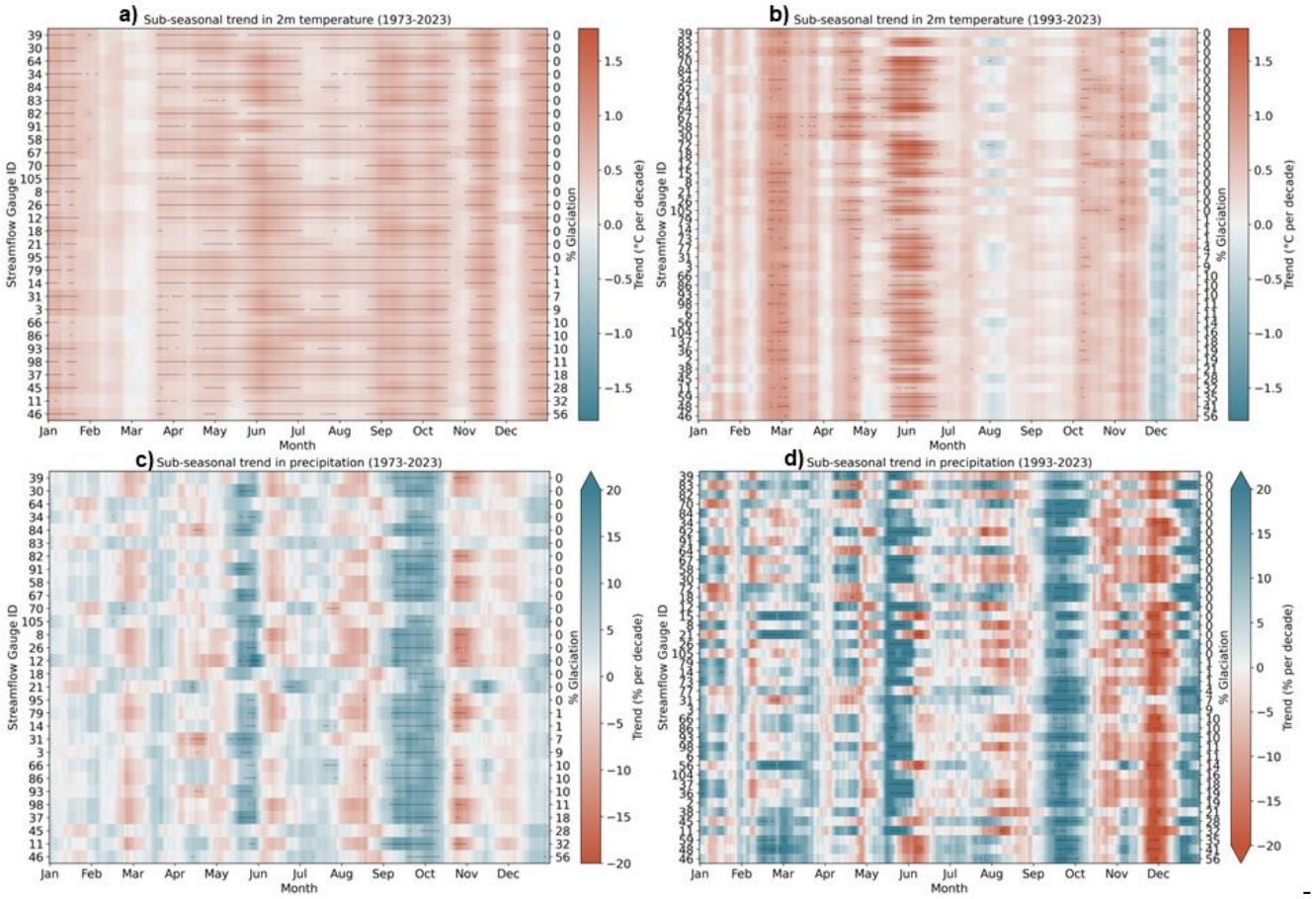

Figure S5: Sub-seasonal trends (21DRM) in catchment-average 2m air temperature (a and b) and precipitation (c and d) from 1973-2023 and 1993-2023. An overlying dashed black line indicates that the trend is significant ($p < 0.05$). Left Y-axis labels show the streamflow gauge ID number. Right Y-labels show the glaciated fraction of the catchment. The data is from the ERA5-Land reanalysis.

Figure S5 shows the sub-seasonal trends in 2m air temperature and precipitation for periods 1 and 2. For air temperature, results for period 1 (Figure S5a) show a predominant significant positive trend in temperature for most of the year. A period in February and March exhibits the smallest (and not statistically significant) trends, along with two shorter periods in October/November and December. Trends in July and August are also small in many catchments. In contrast, results for period 2 show greater variability, including periods with negative trends (Figure S5b). Even though fewer days exhibit statistically significant trends than in period 1, the magnitude of the positive trends is notably larger. Significant increases in temperature are observed in February/March, late April and from late May to late June, while minor decreases are noted in August, December and January.

The precipitation trends present mixed results. For period 1 (Figure S5c), a significant increase in precipitation is evident in May and September and October across almost all catchments. Other parts of the year show limited significance, with slight increases in December and July, and decreases in March, June, August, and November. In period 2 (Figure S5d), statistically significant positive precipitation trends are observed in May and September in most catchments, with slight increases also noted in late December, March, April, late May and July. Decreases are noted in August and early December.

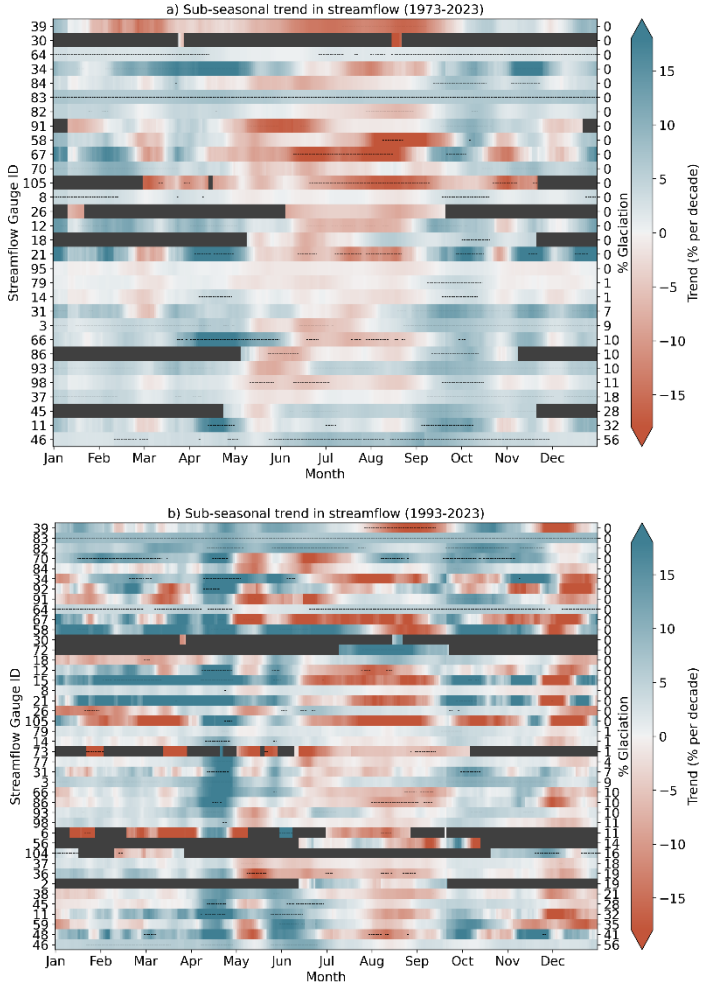

Figure S6: Sub-seasonal trend in streamflow for the periods 1973-2023 (a) and 1993-2023 (b). Colors show the trend in 21-day centered rolling mean streamflow for each day of the year. For periods of the year with insufficient data available, a dark gray color is shown. An overlying dashed black line indicates that the trend is significant. Left Y-axis labels show the streamflow gauge ID number. Right Y-labels show the glaciated fraction of the catchment.

Figure S6 shows sub-seasonal trends in streamflow for periods 1 and 2. The figure shows that for period 1, significant trends (highlighted by dashed black lines) are observed for most gauges for some part of the year, with notable increases observed in winter, spring and fall for most catchments. Negative trends are predominant during the summer season in most catchments,

although positive summer trends are observed in catchments with higher glaciated fractions. Figure S6b, representing the period 1993-2023, exhibits a more pronounced pattern of frequent switches between positive and negative trends, with significant trends being fewer and more scattered throughout the year. Strong increases are particularly evident in April, followed by a decrease in May, indicating a shift in the timing of snowmelt. A strong increase is also evident in September to November. Decreases are observed from June through September for most non-glaciated catchments, and from July through September for many glaciated catchments.

S5 Trends in streamflow

Figure S7 shows trends in annual and summer melt season streamflow in glacial rivers for periods 1 and 2.

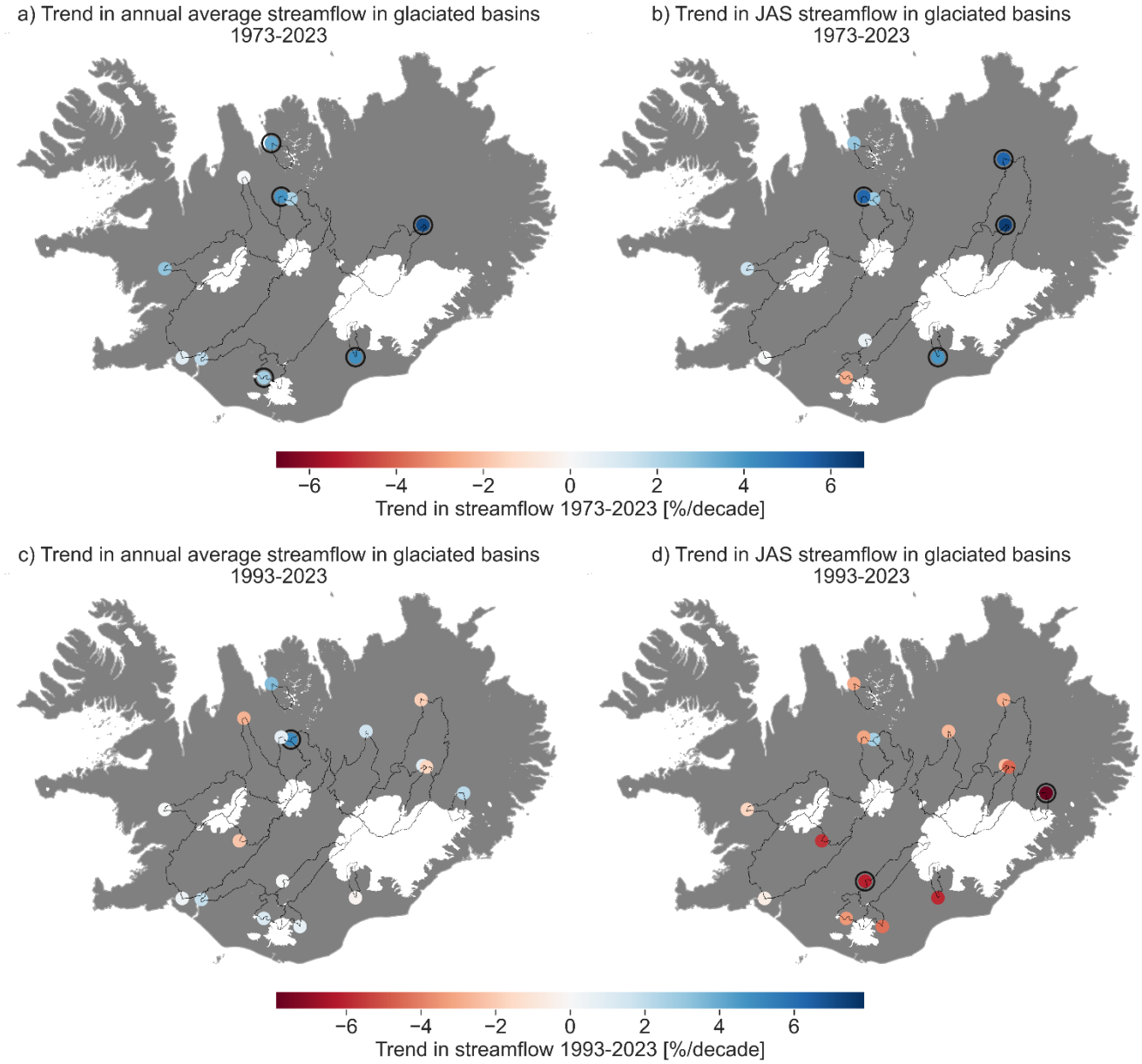

Figure S7: Trends in streamflow for gauges with more than 5% catchment glaciation. Annual trends (a, c) and summer melt season (July, August and September: b, d) in streamflow from 1973-2023 (a, b) and 1993-2023 (b, d). Black circles around gauge markers indicate statistically significant trends ($p < 0.05$). Watershed outlines are shown for each gauge.

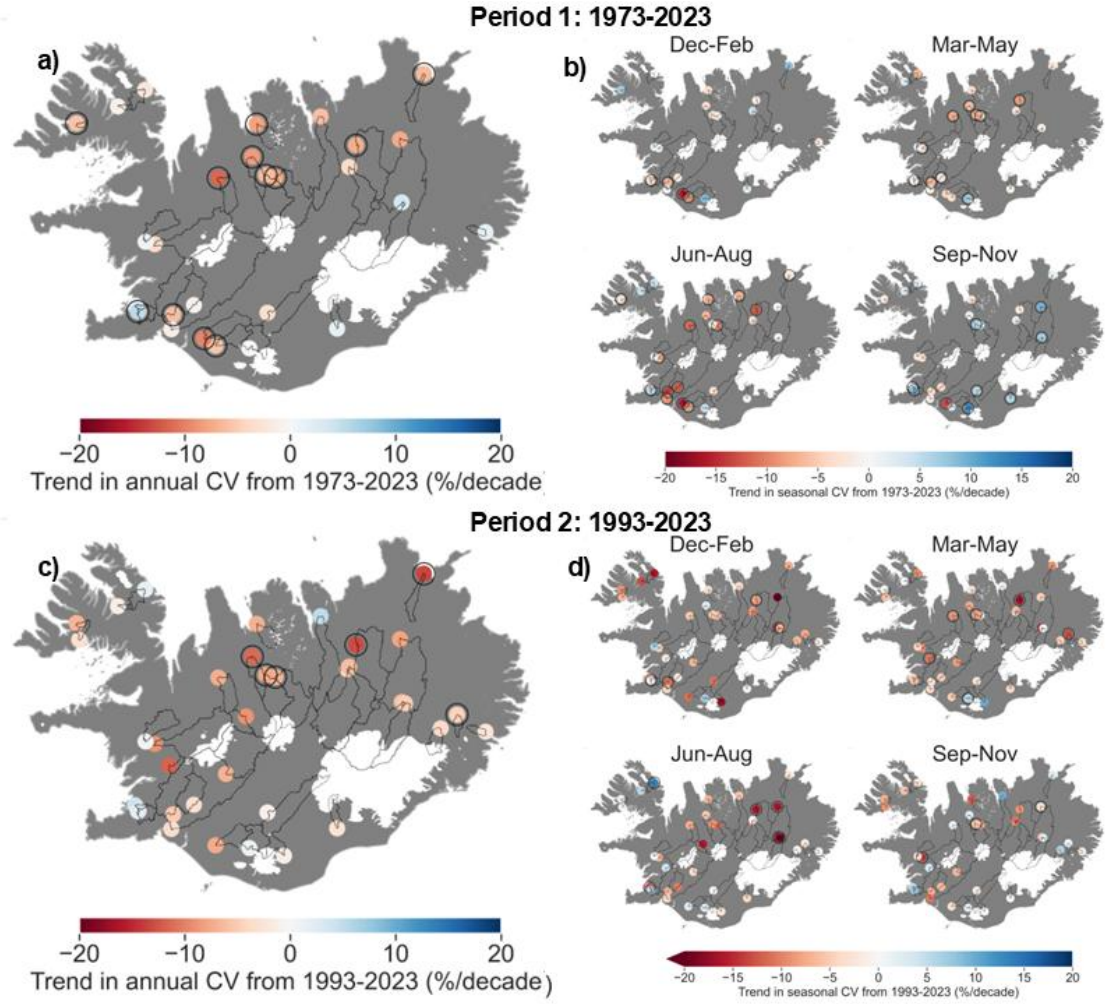

Figure S8: Annual (a, c) and seasonal (b, d) trends in streamflow coefficient of variation (CV) from 1973-2023 (a, b) and 1993-2023 (b, d). Black circles around gauge markers indicate statistically significant trends ($p < 0.05$). Watershed outlines are shown for each gauge.

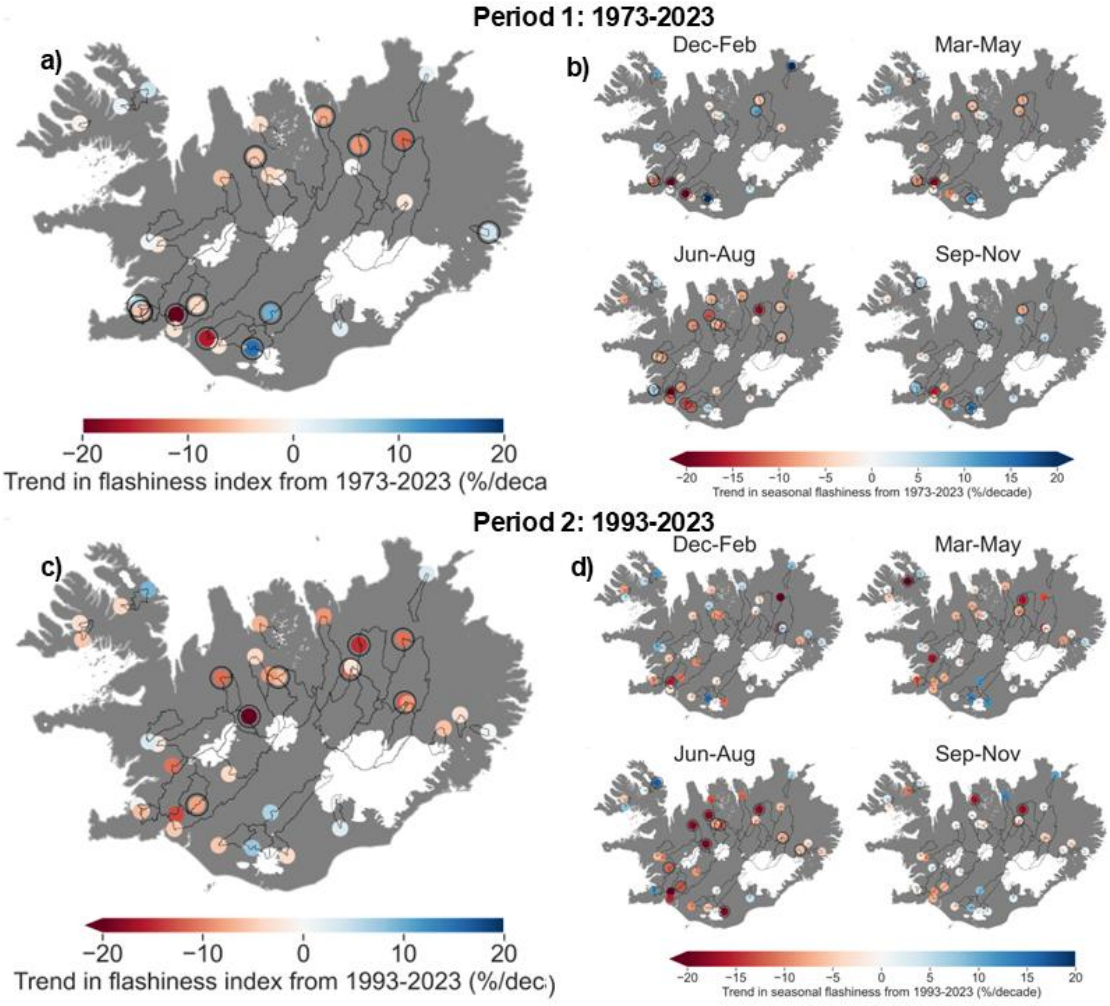

Figure S9: Annual (a, c) and seasonal (b, d) trends in streamflow flashiness index from 1973-2023 (a, b) and 1993-2023 (b, d). Black circles around gauge markers indicate statistically significant trends ($p < 0.05$). Watershed outlines are shown for each gauge.

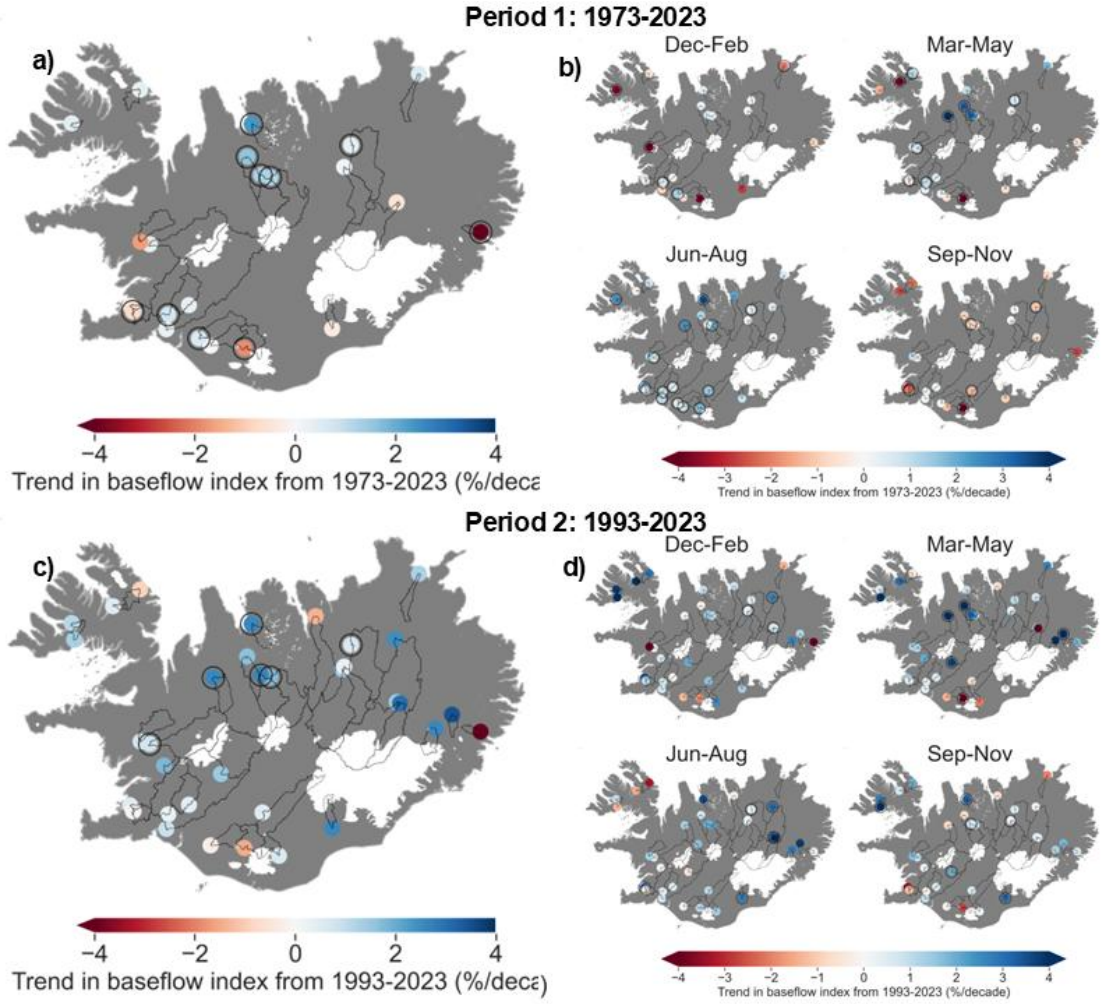

Figure S10: Annual (a, c) and seasonal (b, d) trends in baseflow index from 1973-2023 (a, b) and 1993-2023 (b, d). Black circles around gauge markers indicate statistically significant trends ($p < 0.05$). Watershed outlines are shown for each gauge.

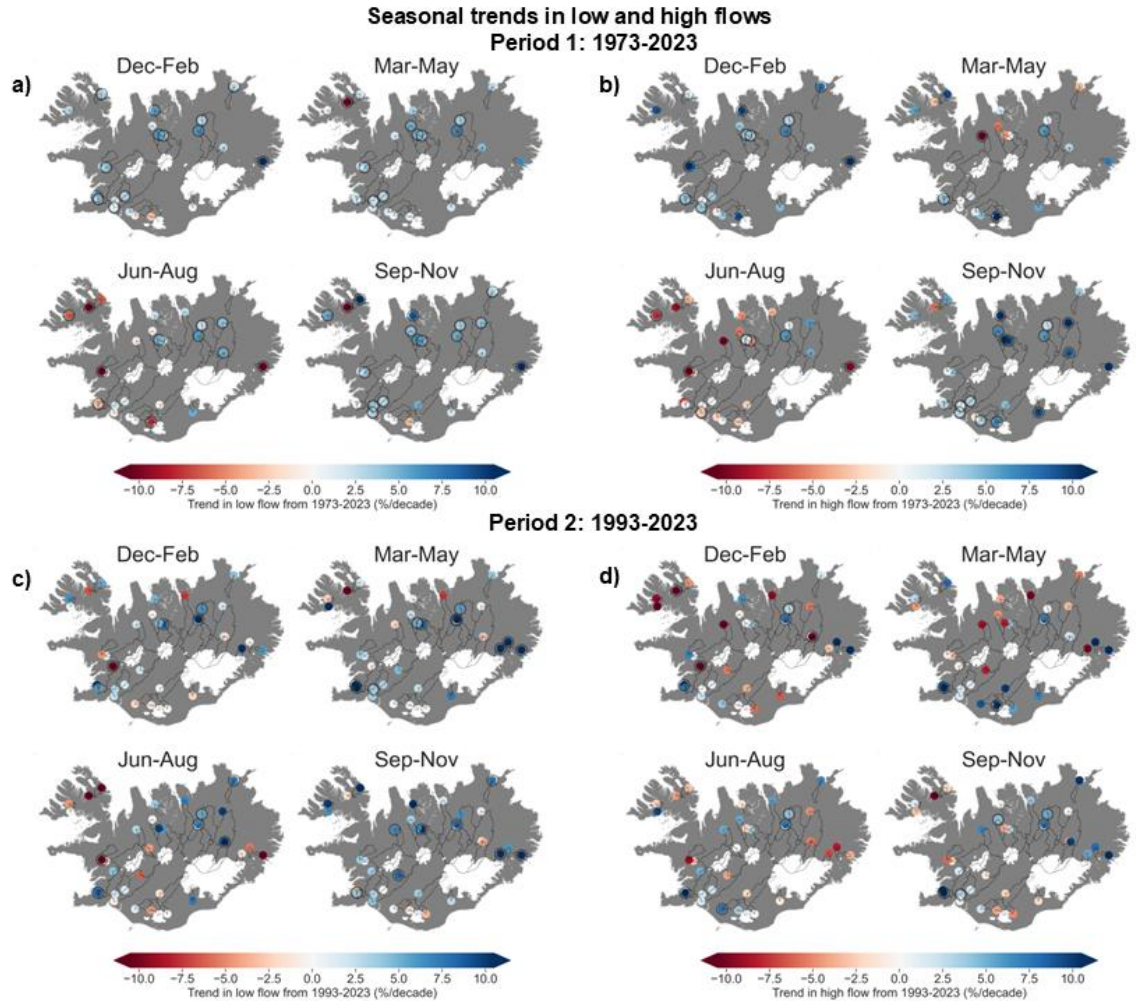

Figure S11: Seasonal trends in low and high flows for periods 1 and 2. Seasonal low (a, c) and high (b, d) flows in streamflow from 1973-2023 (a, b) and 1993-2023 (b, d). Low and high flows are defined as the 10th and 90th percentiles of seasonal flow. Black circles around gauge markers indicate statistically significant trends ($p < 0.05$). Watershed outlines are shown for each gauge.

For period 1, trends in low flows are positive for most gauges in all seasons, particularly in winter, spring and fall. Trends in high flows are positive and significant in most catchments in winter and fall, while summer and spring show mixed results.

For Period 2, seasonal trends in low flows (Figure S11c) remain predominantly positive across most seasons and catchments, particularly in spring and fall, where many gauges show significant increases. Winter trends are more mixed, with both positive and negative changes observed. Summer trends are mixed, with fewer significant results. Trends in seasonal high flows (Figure S11d) are more spatially variable for period 2. Unlike Period 1, winter high flows no longer show widespread increases; trends are now almost evenly split between increases and decreases across gauges. Spring displays a similar pattern, with no dominant trend direction. However, fall continues to show predominantly positive trends. Summer trends remain relatively weak and mostly non-significant, similar to the patterns observed in period 1.

180

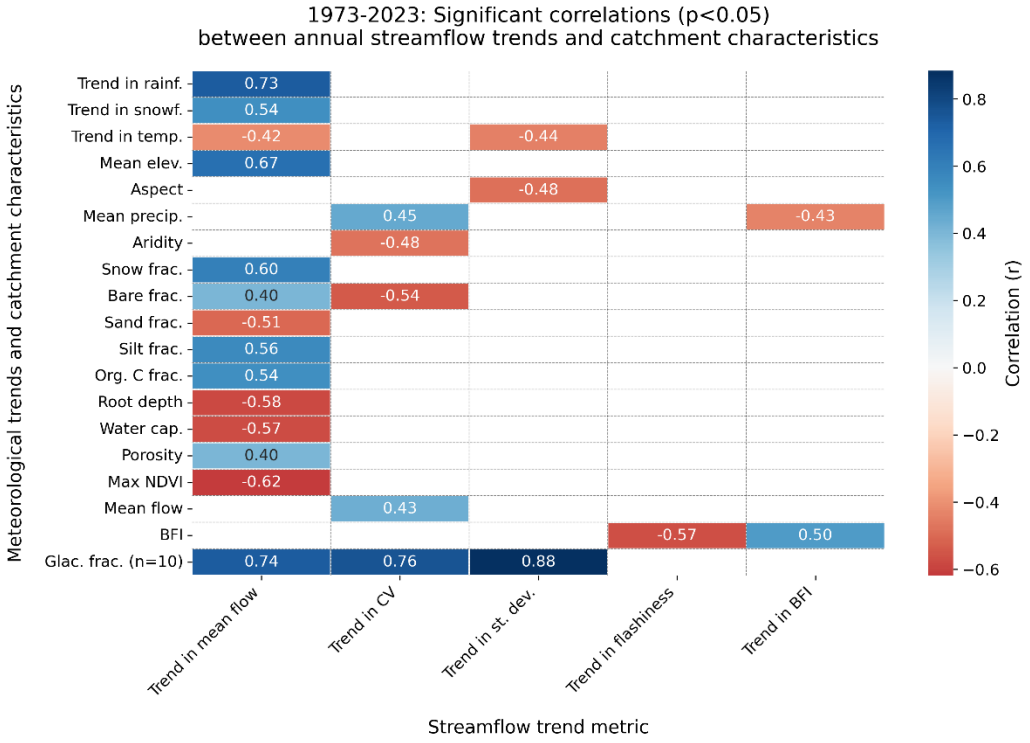

Figure S12: A heatmap showing correlations of annual streamflow metrics with trends in meteorological variables and catchment attributes for the period 1973-2023.

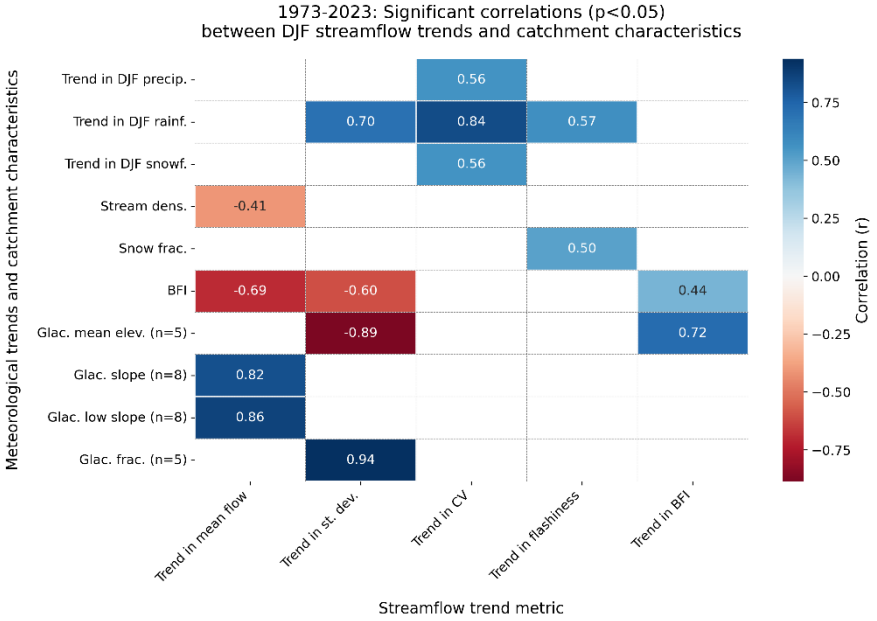

185 **Figure S13: A heatmap showing correlations of winter (DJF) streamflow metrics with trends in meteorological variables and catchment attributes for the period 1973-2023.**

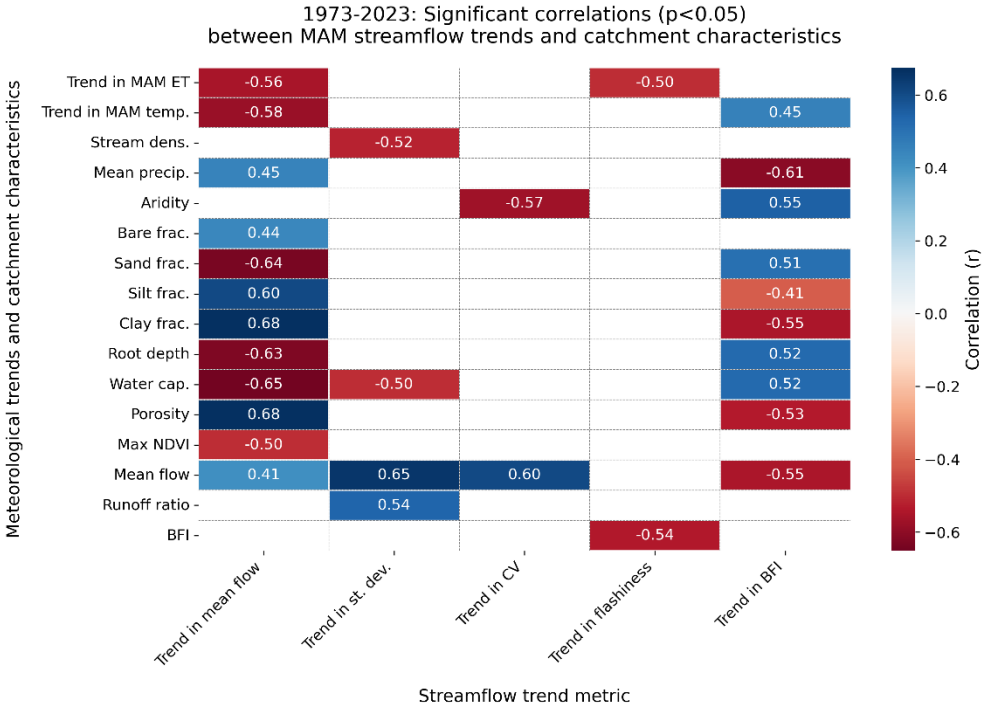

Figure S14: A heatmap showing correlations of spring (MAM) streamflow metrics with trends in meteorological variables and catchment attributes for the period 1973-2023.

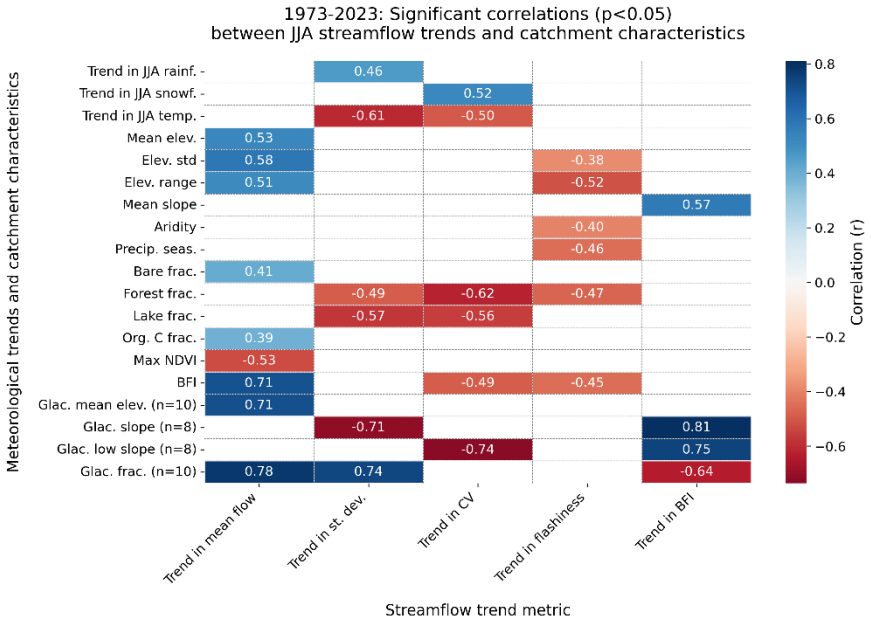

190

Figure S15: A heatmap showing correlations of summer (JJA) streamflow metrics with trends in meteorological variables and catchment attributes for the period 1973-2023.

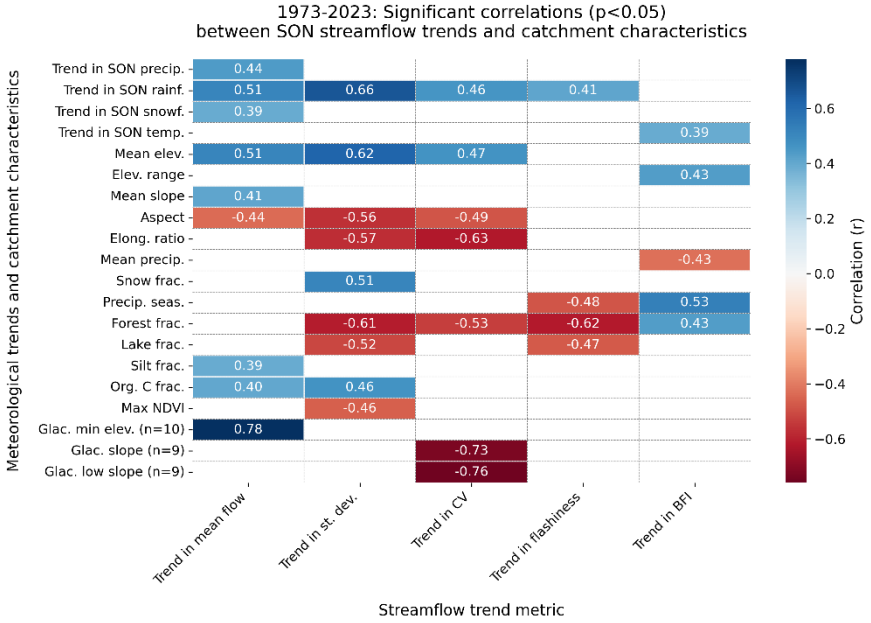

195 **Figure S16: A heatmap showing correlations of fall (SON) streamflow metrics with trends in meteorological variables and catchment attributes for the period 1973-2023.**

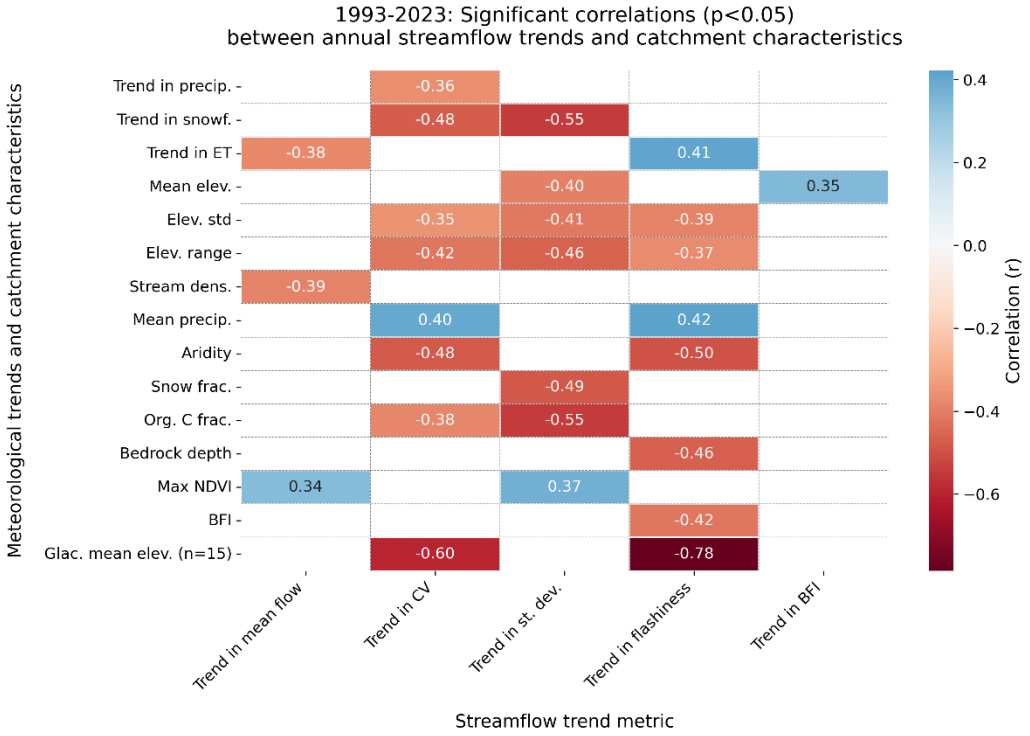

200

Figure S17: A heatmap showing correlations of annual streamflow metrics with trends in meteorological variables and catchment attributes for the period 1993-2023.

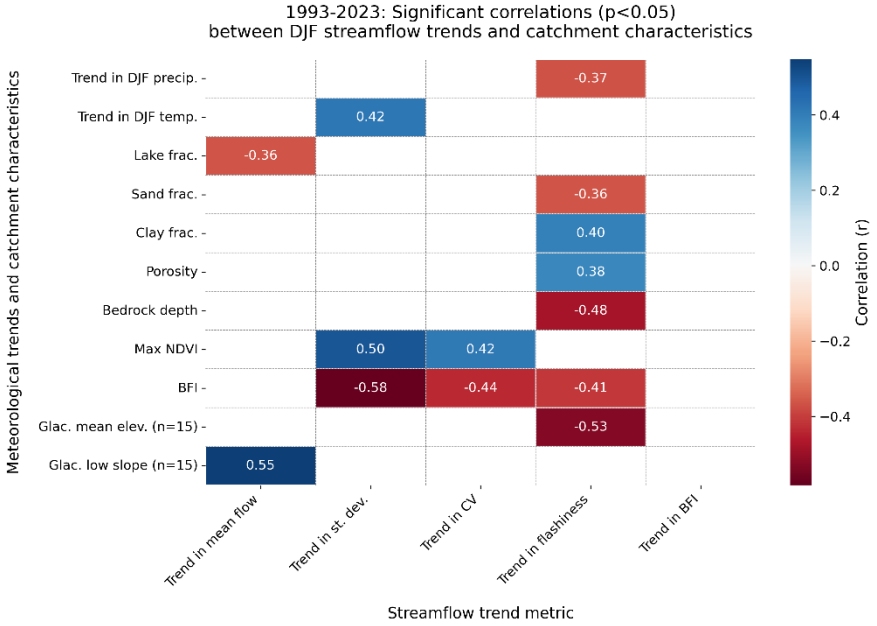

Figure S18: A heatmap showing correlations of winter (DJF) streamflow metrics with trends in meteorological variables and catchment attributes for the period 1993-2023.

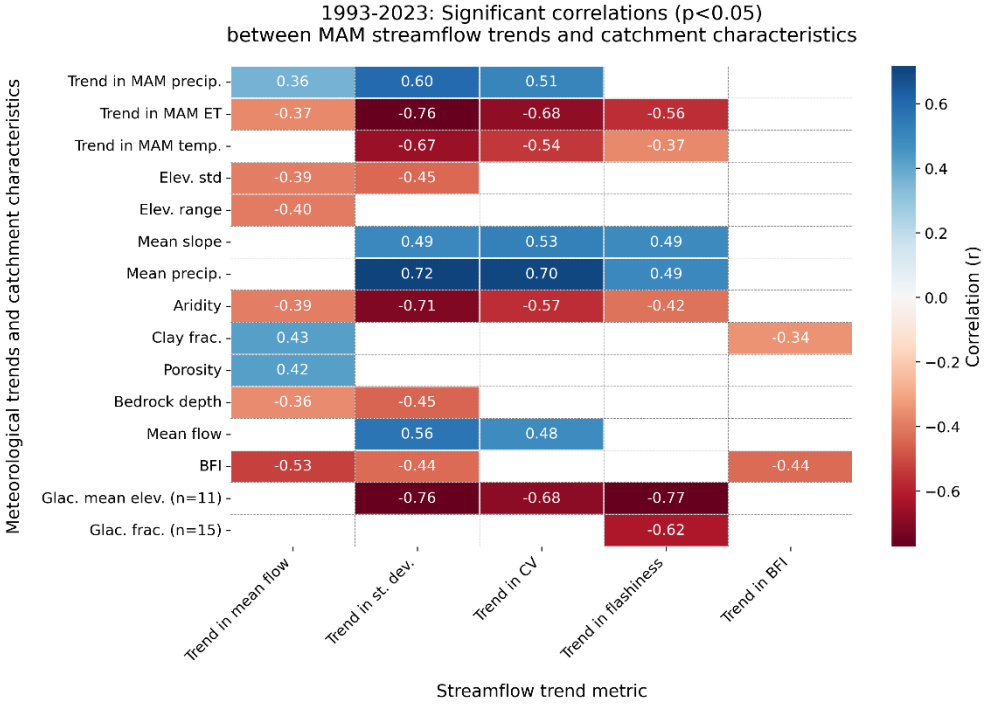

Figure S19: A heatmap showing correlations of spring (MAM) streamflow metrics with trends in meteorological variables and catchment attributes for the period 1993-2023.

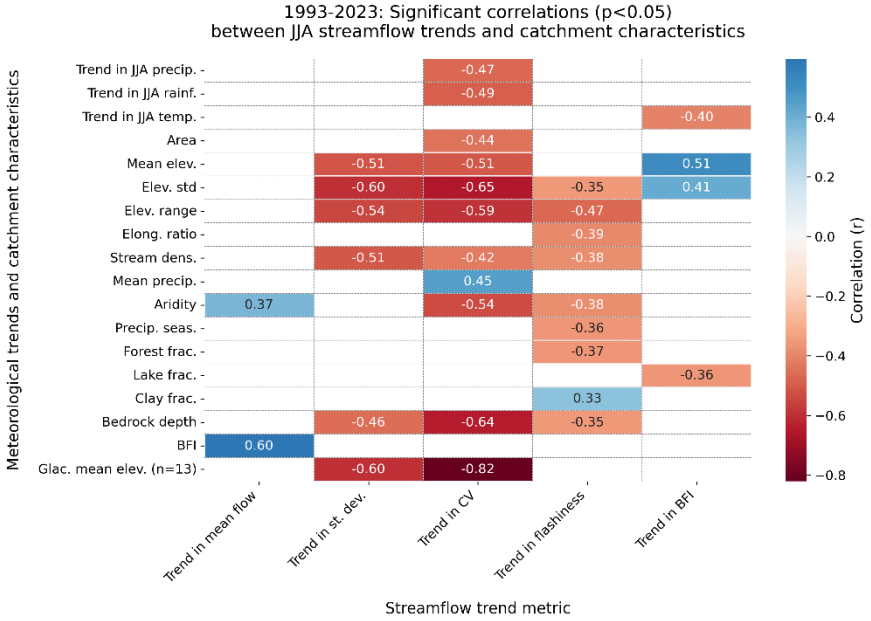

210 **Figure S20: A heatmap showing correlations of summer (JJA) streamflow metrics with trends in meteorological variables and catchment attributes for the period 1993-2023.**

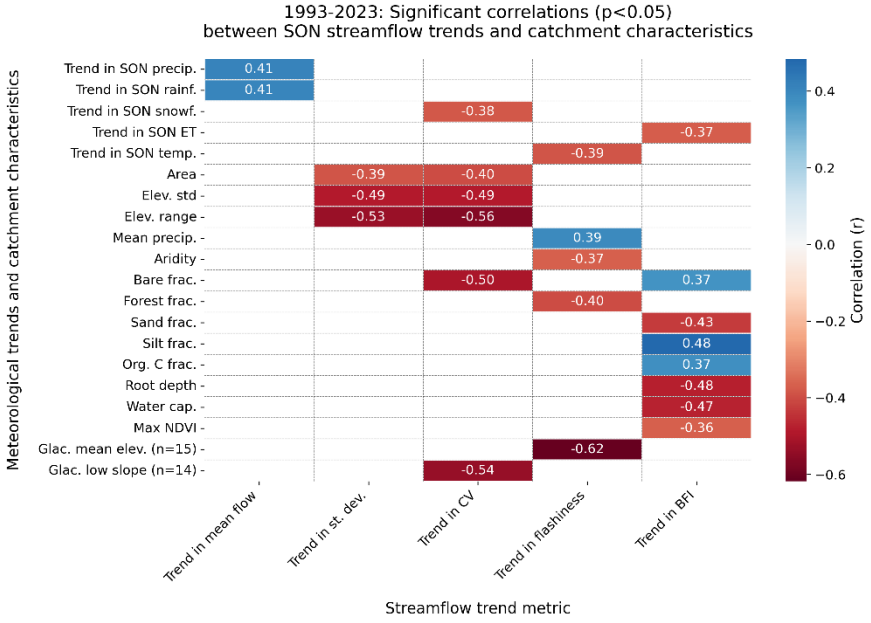

215 **Figure S21: A heatmap showing correlations of fall (SON) streamflow metrics with trends in meteorological variables and catchment attributes for the period 1993-2023.**

S6 Overview of gauges used in the study

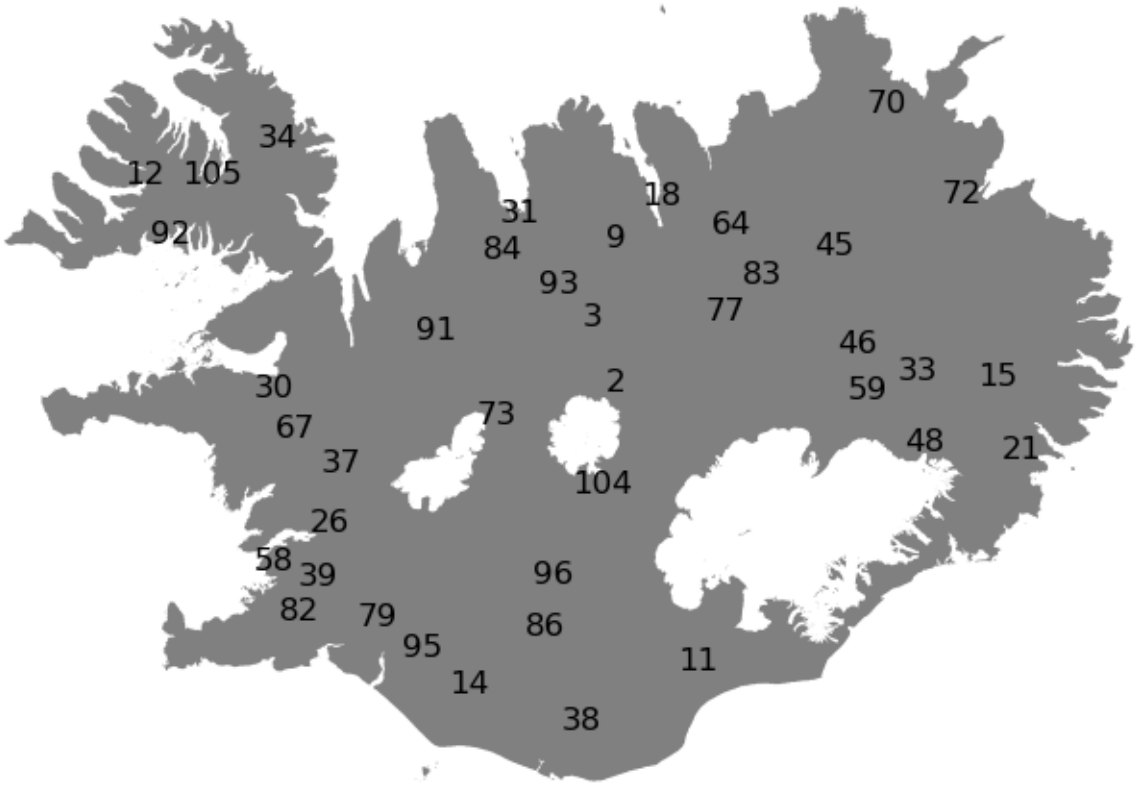

Figure S22: A map showing the location of streamflow gauges from the LamaH-Ice dataset used in the study. Gauges identified by their LamaH-Ice ID numbers.

Table S1: Overview of gauges used in this study, including river names, gauge locations, catchment areas, degree of anthropogenic impact (u: no influence, l: low influence, m: moderate influenc, s: strong influence), catchment glacier percentage and observation periods.

Gauge ID	River name	Station name (location)	Catchment area (km^2)	Degree of anthropogenic impact	Catchment glacier percentage	First year of observations	Last year of observations
3	Austari-Jökulsá	ofan Skatastaða	1134.9	u	8.8	1971	2024
7	Blanda	Langamýri	1673.3	s	10.4	1974	2024

8	Brúará	Dynjandi	642.1	l	0	1948	2023
11	Djúpá	neðan Djúpárdals	226.8	u	33.1	1968	2023
12	Dynjandisá	Sjóarfoss	42.6	l	0	1956	2023
14	Eystri-Rangá	Tungufoss	401.3	l	1.2	1962	2023
15	Fellsá	Sturluflöt II	125.5	u	0	1977	2024
18	Fnjóská	ofan Árbugsár	1129.6	u	0	1976	2023
21	Fossá	Eyjólfsstaðir	113.5	u	0.2	1968	2023
26	Grímsá	Reyðarvatnsós	108.3	l	0	1964	2023
31	Hjaltadalsá	brú, Viðvíkursveit	299.4	u	7	1956	2023
34	Hvalá	Óp	192.8	u	0	1976	2023
36	Hvítá	Fremstaver	1665.1	l	19.4	1985	2021
37	Hvítá	Kljáfoss	1720	u	18.6	1951	2023
38	Hólmsá	Hólmsárfoss	237	u	21.2	1984	2024
39	Hólmsá	Gunnarshólmi	215.5	u	0	1972	2023
45	Jökulsá á Fjöllum	Grímsstaðir	5150.8	u	28.9	1965	2023
46	Jökulsá á Fjöllum	Upptyppingar II	2006.7	u	56.9	1972	2023
48	Jökulsá í Fljótsdal	Eyjabakkafoss	302.4	u	41.5	1985	2024
58	Korpa	Keldnaholt	39.6	l	0	1970	2023
59	Kreppa	Lónshnjúkur	941.8	u	35.9	1985	2023
64	Laxá	Helluvað	1509.7	l	0	1961	2024
66	Markarfljót	Emstrur	516.2	u	10	1982	2023
67	Norðurá	Stekkur	507.4	u	0	1971	2023
70	Sandá	Flögubrú II	265	u	0	1965	2023
73	Seyðisá	Kjölur	301.7	u	1.7	1990	2024
77	Skjálfandafljót	Aldeyjarfoss	1947.9	u	6.1	1987	2023
79	Sog	Ásgarður	997.2	m	1	1972	2024
82	Suðurá	Hófleðurshóll	3.8	u	0	1972	2023
83	Svartá	ofan Ullarfossbrúar	738.8	l	0	1965	2023
84	Svartá	Svartá	390.6	u	0	1932	2023
86	Tungnaá	Maríufoss	1141.1	u	10.2	1959	2024
91	Vatnsdalsá	Forsæludalur	449.7	u	0	1948	2023
92	Vatnsdalsá	Eiði	101.9	l	0	1977	2023
93	Vestari-Jökulsá	Goðdalabrú	842.3	u	10.5	1971	2023

98	Ölfusá	Selfoss	5724.2	l	10.8	1950	2023
102	Þjórsá	Þjórsártún	7437.2	s	12.5	1947	2024
105	Þverá	Nauteyri	44.7	u	0	1967	2021

225

Table S2: Streamflow (Q, m3/s), temperature (T, °C) and precipitation (P, mm/year) averages for periods 1 and 2. Streamflow is measured and temperature and precipiation are derived from the ERA5-Land reanalysis. Note that
230 precipitation is underestimated in ERA5-Land.

Gauge ID	Q1	Q2	T1	T2	P1	P2
3	39.8	40.2	-2.3	-1.8	1045.5	1054.9
7	44.6	44.7	-1.5	-1	1077.2	1084.1
8	66.2	67.5	1.8	2.3	1847.5	1850.8
11	27.4	29.2	-1.4	-1.1	2175.2	2200.9
12	3.1	3.1	-0.2	0.3	1430.3	1433.3
14	20.8	20.6	0.7	1.2	1895.5	1923.1
15		7.7	-1.3	-0.9	1510.2	1542.7
18		38.3	-1.7	-1.3	1098.7	1120.8
21	8.4	8.7	-0.1	0.3	1666.9	1711.6
26		5.6	-0.2	0.3	1605.6	1614.3
31	11.2	11.4	-1.7	-1.2	1169.7	1186.5
34	14.8	15	0	0.4	1357.8	1381.6
36		86.6	-1.5	-1.1	1453.2	1457.4
37	82.6	85.4	-1.2	-0.8	1317.6	1326.2
38		36.9	0.2	0.6	2422.9	2480.7
39	2.1	1.9	2.1	2.6	1526.9	1544.3
45		188.6	-2.4	-2	1238.5	1252.1
46	96.3	101.6	-3.8	-3.5	1421.5	1435.7
48		26.9	-2.5	-2.1	1662	1691.3
58	1.5	1.4	2.4	2.8	1453.9	1467.6
59		45.3	-3	-2.6	1457.5	1473.5
64	38	38.7	-0.6	-0.1	1015.8	1030.1
66	43	43.7	-0.3	0.1	2173.6	2211.8
67	21.8	21.6	0.7	1.2	1163	1176.4
70	13.7	13.9	0.4	0.8	1083.7	1098
73			-1.6	-1.1	1160	1166
77		49.4	-2.2	-1.8	1133.8	1145.5
79	108.5	108.5	1	1.5	1675.5	1684.8

82	0.4	0.4	2.7	3.1	1461.4	1476
83	21.6	22.5	-1.5	-1	1127.9	1144.3
84	10.2	10.2	-0.5	0	974.6	982.6
86		87.8	-0.8	-0.3	1695.2	1719.2
91		9.1	-0.5	0	987.1	1000.9
92		7.1	0.1	0.6	1455.5	1457.5
93	22.7	23.6	-1.9	-1.4	1024.1	1030.4
98	377.4	378.1	0.3	0.7	1642.5	1648.2
102	350.2	353.4	-1	-0.5	1446.2	1457.7
105		2.4	-0.1	0.3	1315.5	1334.5

References

Fleig, A. K., Andreassen, L. M., Barfod, E., Haga, J., Haugen, L. E., Melvold, K., Hisdal, H., and Saloranta, T.: Norwegian Hydrological Reference Dataset for Climate Change Studies, Norwegian Water Resources and Energy Directorate, Oslo, Technical report, ISBN: 978-82-410-0869-6, 2013.

Hussain, M. M., Mahmud, I., and Bari, S. H.: pyHomogeneity: A Python Package for Homogeneity Test of Time Series Data, J Open Res Softw, 11, https://doi.org/10.5334/JORS.427, 2023.

Ladson, A. R., Brown, R., Neal, B., and Nathan, R.: A standard approach to baseflow separation using the Lyne and Hollick filter, Australian Journal of Water Resources, 17, 25–34, https://doi.org/10.7158/W12-028.2013.17.1, 2013.

Pettitt, A. N.: A Non-Parametric Approach to the Change-Point Problem, J R Stat Soc Ser C Appl Stat, 28, 126–135, https://doi.org/10.2307/2346729, 1979.